# Local charge-density-wave structure in 1$T$-$TaS_2$ determined by scanning tunneling microscopy

R. E. Thomson, U. Walter,* E. Ganz, J. Clarke, and A. Zettl
*Department of Physics, University of California, Berkeley, California 94720*
*and Center for Advanced Materials, Lawrence Berkeley Laboratory, Berkeley, California 94720*

P. Rauch and F. J. DiSalvo
*Department of Chemistry, Baker Laboratory, Cornell University, Ithaca, New York 14583*
(Received 2 May 1988)

We have imaged simultaneously the lattice and the charge-density-wave (CDW) superstructure in 1$T$-$TaS_2$ over the temperature range 370–77 K. In the nearly commensurate (*NC*) phase between 353 and 183 K we find that the CDW occurs not in commensurate domains but with a uniform, incommensurate orientation throughout the crystal surface. Local measurements of the relative angle between the CDW and the underlying atomic lattice failed to find any areas where the local angle was the commensurate angle, in contradiction to the hexagonal-domain *NC*-phase model of Nakanishi and Shiba. In the nearly commensurate triclinic (*T*) phase between 223 and 283 K produced when the temperature is increased, we have directly observed CDW discommensurations in agreement with the stretched honeycomb discommensurate *T*-phase model of Nakanishi and Shiba.

## I. INTRODUCTION

One of the most interesting structural phase transitions is that which involves the formation of charge-density waves (CDW) in low-dimensional metals. Substantial Fermi-surface nesting can lead to divergences in the dielectric response function at a wave vector **q** which spans large portions of the Fermi surface. These divergences are in turn transferred, via the electron-phonon interaction, to the phonon spectrum itself, creating a soft phonon mode. The result is a stable, gapped Fermi surface and a frozen-in phonon of wave vector **q**, with a corresponding modulation of the electronic density of states and charge density in real space. If **q** is unrelated to the original lattice periodicity, the CDW will in general not be commensurate with the underlying atomic lattice.

CDW's are observed in a host of quasi-one-dimensional and quasi-two-dimensional conductors, and have been studied extensively by diffraction,[1] transport,[2] and elasticity[3] techniques. Since the CDW distortion also results in a modulation of the density of states near the Fermi level, CDW's are well suited for study by scanning tunneling microscopy. The tunneling current of a scanning tunneling microscope (STM) is directly proportional to the density of states at the Fermi level; hence the STM can image both the underlying atomic lattice and the real-space CDW superstructure on a crystal surface. The ability of a STM to image a CDW was first demonstrated by Coleman *et al.*[4] for the quasi-two-dimensional metals 1$T$-$TaS_2$ and 2$H$-$TaSe_2$. More recent STM results[5] show both the underlying atomic lattice and the CDW imaged simultaneously in related CDW materials.

In principal, the STM technique can be used to study real-time CDW formation, the CDW order parameter (amplitude), local registration (commensurability) with the atomic lattice including domain structure and discommensurations, polarization distortions, and metastable states, and, in the case of a sliding CDW condensate, CDW dynamics. We have used the STM to study in detail the static, temperature-dependent CDW structure in 1$T$-$TaS_2$ over a wide temperature range. As a function of temperature, five different phases are known to exist in this compound,[6] four of which support a CDW. The spacing and orientation of the CDW superstructure with respect to the lattice is different in each phase. Our method produces images showing both the lattice and the CDW in the different phases, enabling us to determine the local registration of the CDW. Our results resolve longstanding questions regarding discommensurations and domain structure in 1$T$-$TaS_2$.

## II. STRUCTURAL PHASES OF 1$T$-$TaS_2$

At temperatures above 543 K no CDW exists in 1$T$-$TaS_2$. When cooled, the material first enters the incommensurate (*I*) phase (543–353 K). Further cooling brings the sample into the nearly commensurate (*NC*) phase (353→183 K), and finally into the commensurate (*C*) phase ($T<183$ K). The material is strongly hysteretic and on warming again one obtains the nearly commensurate triclinic (*T*) phase (223→283 K) followed by a transformation back to the *NC* phase at 283 K. Recent experiments on thermal expansion,[7] atomic beam diffraction,[8] x-ray diffraction,[9] heat capacity,[10] elastic constants,[11] and transport properties[6,12,13] have shown that the *T* phase is distinct from the *NC* phase. Table I summarizes the temperature ranges of these phases and their important characteristics.

The CDW is concomitant with a periodic lattice distortion. The lateral lattice displacements are on the or-

 

der of 0.2 Å,[14] which is below the lateral resolution of an STM. This lattice shift can be studied on x-ray diffraction,[9,15,16] electron diffraction,[1,15,17,18] convergent beam electron diffraction,[19,20] low-energy electron diffraction,[21] and atomic beam diffraction.[22] In the past, these diffraction techniques along with high-resolution electron microscopy (HREM)[17,23] have been the major methods which have given insight into the detailed structure of the different phases of the CDW on the atomic scale. For the *NC* and *T* phase of 1$T$-$TaS_2$, diffraction techniques have proven indispensable in providing basic data to determine the quite complicated temperature-dependent structure.[9,24] However, there is still the open and challenging question of how these two phases are actually arranged on an atomic scale within a sublayer, i.e., whether they are continuously incommensurate,[15] or form a domainlike discommensurate structure, in which the CDW is commensurate within a single domain and is incommensurate only over a finite width at the domain boundary, as proposed by Nakanishi and Shiba.[25,26]

McMillian proposed a theory of discommensurations for the incommensurate phases of CDW's.[27] Nakanishi and Shiba[25,26] later extended this theory to the specific case of 1$T$-$TaS_2$, proposing the hexagonal-domain model for the *NC* phase and the stretched honeycomb model for the *T* phase. In addition to the original x-ray diffraction results,[9,24,25] the major piece of experimental evidence supporting both discommensuration models is the x-ray photoemission experiment of Hughes and Pollack.[28] These authors showed that the x-ray photoemission spectroscopy of the 4$f$ lines of the Ta atoms are split, indicating two inequivalent sites for the Ta atoms, a result that does not obviously occur if the CDW is uniformly incommensurate. However, the two HREM studies that achieved atomic resolution on the *NC* phase of 1$T$-$TaS_2$ reported that the CDW is locally incommensurate[17,23] in contradiction with the discommensuration theory of Nakanishi and Shiba.

In a similar material, 2$H$-$TaSe_2$, several groups have performed extensive electron diffraction and dark-field transmission electron microscopy (TEM) studies.[29] They have shown that 2$H$-$TaSe_2$ does exhibit discommensurations in its CDW in at least two phases and that the exact geometrical configuration depends on the thermal history of the sample. However, the scale of the discommensurations which were directly observed in 2$H$-$TaSe_2$ is somewhat larger ($>300$ Å) than those predicted in 1$T$-$TaS_2$ (50–100 Å).[25,26] Thus the predicted discommensurations in 1$T$-$TaS_2$ are below the resolution of dark-field TEM (Ref. 20) and have never been directly verified.

In an effort to shed some light on this controversial problem, we have performed an STM experiment on 1$T$-$TaS_2$ between 77 and 370 K. We are able to observe the surface CDW as well as the atomic lattice over large areas. In the *NC* phase, we find that the CDW is not arranged in commensurate domains, but occurs at a constant, incommensurate orientation throughout the surface. The angle of the orientation of the CDW relative to the lattice was measured locally and found to vary continuously with temperature, as reported by Scruby *et al.*[15] However, in the *T* phase, we do observe discommensurations very similar to those predicted by Nakanishi and Shiba.[26]

## III. EXPERIMENTAL CONFIGURATION

### A. Sample preparation

Samples were prepared from Ta powder (99.9%-pure Wah Chang) and S (99.9999%-pure Atomergic Chemetals) in stoichiometric amounts sealed in quartz tubes (200-mm long, 16-mm i.d.) along with 58 mg of excess S

TABLE I. The phases of 1$T$-$TaS_2$.

| Phase | Temperature | $\phi$ (deg) | Comments |
|---|---|---|---|
| Normal | above 543 K | | No CDW is known to exist. Difficult to study because it transforms slowly to 2$H$ polytype. |
| *I* | 543–354 K | 0 | CDW is uniformally incommensurate but is aligned with the lattice. |
| *NC* | 353–183 K upon cooling and 283–353 K upon warming | 11.6 at 331 K to 13.1 at 250 K | CDW is incommensurate and rotated away from the lattice. Discommensurate hexagonal-domain structure proposed by Nakanishi and Shiba. |
| *C* | below 183 K upon cooling and below 223 K upon warming | 13.9 | CDW is uniformly commensurate. |
| *T* | 223–283 K upon warming | 12–13 | CDW is incommensurate and does not exhibit threefold symmetry. Discommensurate stretched honeycomb domain structure proposed by Nakanishi and Shiba. |

(approximately 1 $\mu g/mm^3$ of tube volume) and 100 mg of iodine. After the tubes were slowly heated to 550 °C, and examined for complete reaction of the tantalum with the sulfur, they were heated to 900 °C to complete the formation of $TaS_2$. Single crystals of the 1*T* polytype were grown by placing the tubes in a temperature gradient from 843 to 768 °C for three weeks. The tubes were then rapidly quenched in water to retain the 1*T* polytype, and the crystals washed three times with dichloromethane to remove any residual iodine.

### B. Microscope operation

The tunneling microscope used for this experiment is a modification of designs by Kaiser and Jacklevic,[30] and by Drake *et al.*[31] It consists of an aluminum plate, supported by three screws, clamped onto the main microscope body by two springs (Fig. 1). Two screws at one end of the plate control the coarse positioning of the sample, which is mounted on the plate. Because the line joining the pivot points of these screws is offset from the tip by 1.5 mm, adjustment of the third screw, 30 mm from the tip, causes a motion of the sample relative to the tip of 20 $\mu$m per turn. We achieve *x-y* scanning by applying differential voltages to a piezoelectric tube scanner[32] with the tip mounted in the center. We use $Pt_{0.8}Rh_{0.2}$ tips, which we form simply by cutting the wire with blunt wire cutters.

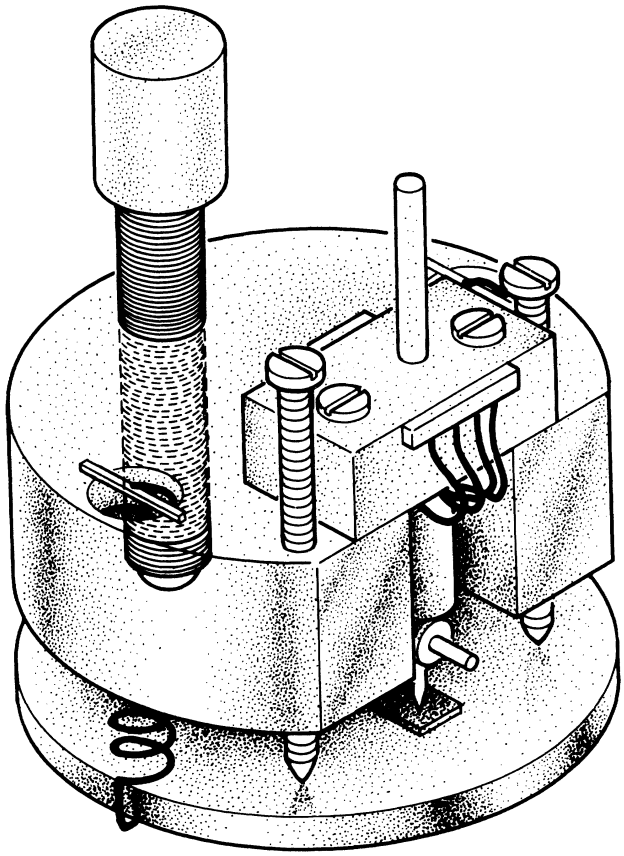

FIG. 1. Schematic drawing of the STM. The thin plate acts as a lever arm to facilitate adjustment of the sample to within tunneling range. The fine-adjust screw is controlled by a motor and the entire microscope can be immersed in a cryogenic liquid.

We adjust the coarse position of the sample under a low-magnification microscope, moving the tip to within about 50 $\mu$m of the surface. We use a motor to turn the fine-adjust screw, bringing the tip towards the sample with the *z*-drive feedback circuit in operation. As soon as a tunneling current is detected, the *z* drive retracts and the motor is switched off automatically. In this way, we can bring the tip within working range of the sample without touching the two together.

Extending the technique of Drake *et al.*[33] who imaged samples immersed in oil, we cleave single crystals of 1*T*-$TaS_2$ under mineral oil before mounting them in the STM. The entire microscope is then lowered into a thin-walled copper can filled with reagent grade *n*-pentane. The pentane dissolves the oil, thus producing a surface which has never been exposed to air and which can be cooled to 150 K. However, for samples to be imagined at 77 K we cleave the sample in air and do not use *n*-pentane inside the can.

We lower the copper can into a dewar containing either an ice bath of *n*-pentane (143 K) or liquid nitrogen. In the case of the *n*-pentane, the temperature of the experiment can be adjusted between 150 and 295 K by allowing the bath to warm slowly back to room temperature over a period of several hours. This technique allows the temperature of the experiment to drift slowly ($\approx$3 °C/h) while the data are taken, but in most cases this does not significantly degrade the quality of the images. The temperature of the sample is measured with a silicon switching diode (1N-4448) mounted directly behind the sample. For experiments run above room temperature, we substituted a bath of mechanical pump oil for the pentane and used a heating tape to adjust the bath temperature.

We acquire data in the constant height, or current imaging mode,[34] taking one complete image in about 2 sec. We find that this technique is superior to the constant current, or topographic mode for this material because it allows us to image the atomic lattice simultaneously with the CDW. This is a critical requirement when one wishes to determine the angle of orientation of the CDW with respect to the lattice. Generally, we post process the raw data to enhance the resolution of the CDW and the lattice (see the Appendix).

We believe that the CDW structure we observe is identical to the undisturbed CDW structure, although we are applying a small (0.1–20 mV) bias voltage between the surface and the scanning tip. Tunneling studies[35] of 1*T*-$TaS_2$ showed that the CDW gap is about 0.1–0.5 V over the 77–320 K temperature range. We can safely assume, therefore, that the tunneling current is only a small perturbation to the static CDW. This conclusion is further supported by the fact that the STM images do not depend significantly on the amplitude or polarity of the bias voltage.

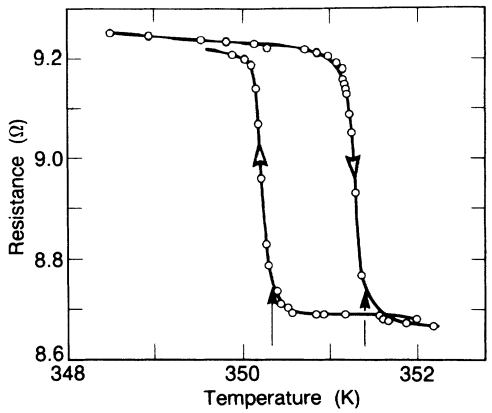


FIG. 2. Measured resistivity of 1$T$-$TaS_2$ around the transition at 350 K. Two vertical arrows indicate the temperature at which the transition was observed in the STM.

## IV. RESULTS AND DISCUSSION

### A. *I* phase to *NC* phase

We have studied the transition from the $I$ to the $NC$ phase with care because the rather large rotation ($\phi \approx 11°$) of the **q** wave vector of the CDW relative to the lattice enables one to observe the transition in real time. This transition is quite dramatic since in the $I$ phase **q** is aligned with the hexagonal lattice so that the rotation of the CDW superstructure is observed directly.

In Fig. 2 we show the measured resistivity of our sample around the transition. In accordance with previous transport measurements[13] we find that the resistivity shows a small but significant hysteresis of 2 K at the transition. In Figs. 3(a) and 3(b) we display the raw and filtered data taken well above the transition. Figures 3(c) and 3(d) show the raw and filtered image taken just below the transition. The underlying atomic lattice is clearly visible and thereby serves as a reference for the CDW. We find that after the transition the CDW has rotated by 10.9° relative to its position before the transition. To determine whether the surface transition occurs at the same temperature as the bulk transition we have also studied the transition for both increasing and decreasing temperature, continuously monitoring any changes in the CDW structure relative to the lattice, while simultaneously measuring the bulk resistivity. We were able to capture the surface transitions, indicated in Fig. 2 by the vertical arrows, to within a few hundredths of a kelvin. Obviously, the differences between the bulk and surface transitions are very small, comparable to our estimates of temperature gradients between the sample and thermom-

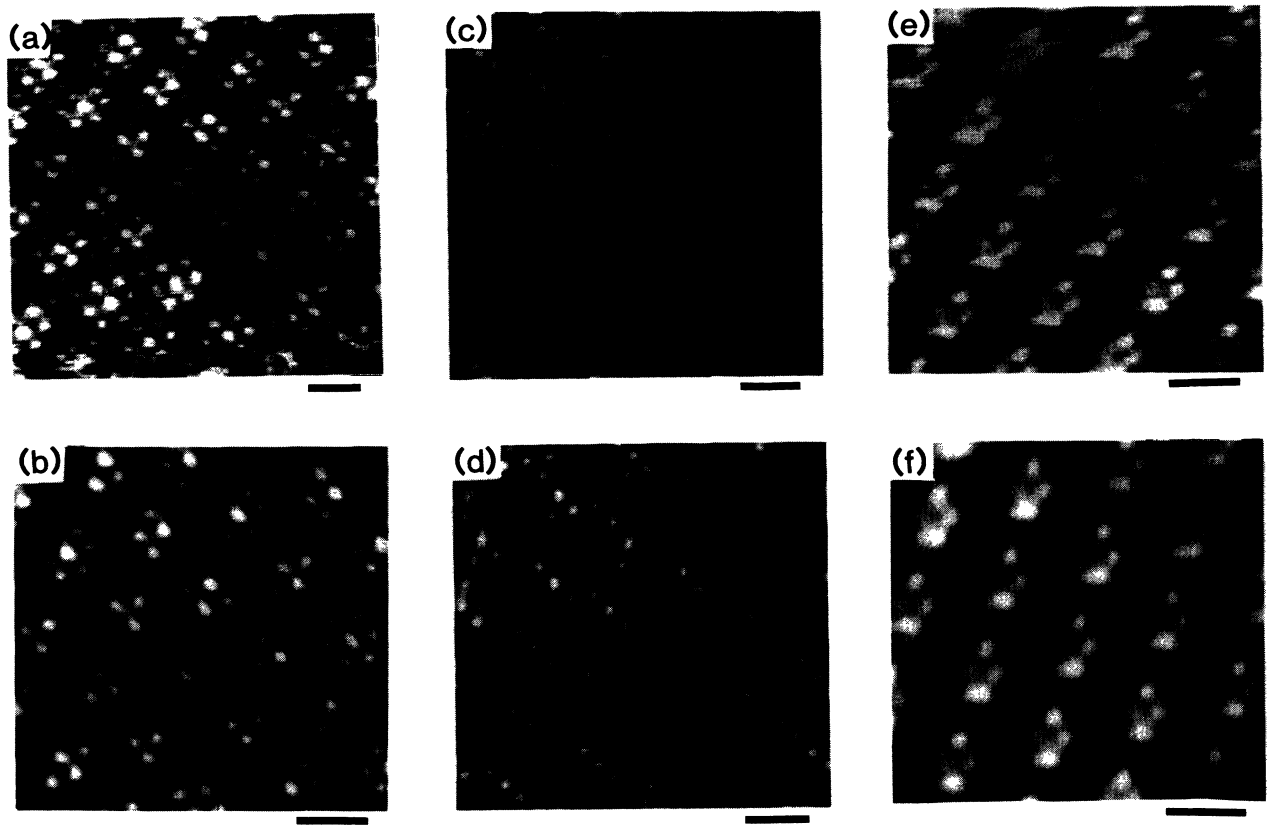


FIG. 3. Raw data and filtered images of 1$T$-$TaS_2$. The bar below each picture is 10 Å. (a) Raw and (b) low-pass filtered image taken at 360 K in the $I$ phase. The image was taken in air with 7.5-nA tunneling current and the sample biased at −4.8 mV. (c) Raw and (d) filtered image taken at 350 K just after the transition to the $NC$ phase. The sample was under silicone oil and the image was taken with 5-nA tunneling current and the sample biased at −13 mV. (e) Raw and (f) filtered image taken at 143 K in the $C$ phase. The sample was immersed in $n$-pentane and the image was taken with 5-nA tunneling current and the sample biased at + 20 mV.

eter. We therefore conclude that the nature of the transition is the same at the surface as in the bulk, suggesting that the CDW structures should be identical.

### B. *C* phase

Before discussing the more interesting *NC* and *T* phases, we present results on the *C* phase ($T < 183$ K), to which the *NC* and *T* phases are closely related. Figures 3(e) and 3(f) display the raw and filtered data taken at 150 K. Again, both the CDW and the underlying lattice are visible. Moreover, it is evident that the CDW is commensurate with the lattice, since the lattice structure within each CDW maxima appears to be identical.

In the *C* phase as well as the other CDW phases we find that the CDW supercell can be rotated counterclockwise ($\alpha$ rotated in the notation of Wilson *et al.*[1]), as it is in Fig. 3(e), or clockwise ($\beta$ rotated), relative to the lattice. It is well known from x-ray diffraction experiments that these two related superstructures can coexist in the same sample. On one occasion we found adjacent areas of $\alpha$ and $\beta$ rotation, but were unable to image the domain boundary. In all other cases, we have observed only one type of rotation across the entire surface area accessible to our microscope (about 1 $\mu m^2$).

### C. *NC* phase

The comprehensive study by Scruby *et al.*[15] suggested that in the *NC* phase the CDW forms a structure where the component of the wave vector **q** parallel to the basal plane is almost, but not quite, commensurate with the lattice. Between 331 and 250 K, $\phi$, the angle of rotation of the CDW with respect to the lattice was found to change continuously from 11.6° to 13.1°, 13.9° being the angle of a commensurate CDW.

Inspired by the finding of higher-order harmonics of the fundamental CDW wave vector by advanced x-ray techniques, Nakanishi and Shiba[25,26] proposed a domain-like discommensurate (DC) CDW structure for both the *NC* and *T* phases. They suggested that in the *NC* phase a honeycomb domain structure with domains having an estimated diameter of $20a_0$ to $25a_0$ ($a_0 = 3.346$ Å is the lattice constant) and a diffuse domain boundary supercedes the CDW structure and is responsible for the higher-order harmonics. In contrast to the interpretations of Scruby *et al.*,[15] the CDW in this case should be commensurate within a given domain. From the even more detailed x-ray report on asymmetric satellite reflection in the *T* phase[9] they concluded that this honeycomb domain superstructure is squeezed into a triclinic $3 \times 1$ stretched honeycomb domain superstructure[26] of roughly the same size. Later, Tanda and Sambongi described the stretched honeycomb structure in more detail.[9]

Given these detailed experimental results and theoretical predictions we have imaged the CDW structure in the *NC* phase at various temperatures to determine the correct model. The STM is the ideal instrument to distinguish between the models of Nakanishi *et al.*[25,26] and Scruby *et al.*[15] because it can image the CDW locally. Although the difference between the incommensurate angle and the commensurate angle is relatively small, ranging from about 1° to 3°, we would expect to be able to see the commensurate domains from a visual inspection of the raw data: When the CDW is commensurate each CDW maximum (or minimum) contains an identical array of atoms. This commensuration is confirmed in pictures published by Giamgattista *et al.*[5] of the commensurate phase of 4*Hb*-$TaSe_2$ as well as by our own data at 143 K [Fig. 3(f)]. However, our images in the *NC* phase do not show any regions where the CDW maxima appear identical. This dissimilarity can be seen clearly in Fig. 4, a typical filtered image of the *NC* phase at room temperature. Figure 3(d) serves as a second example. The

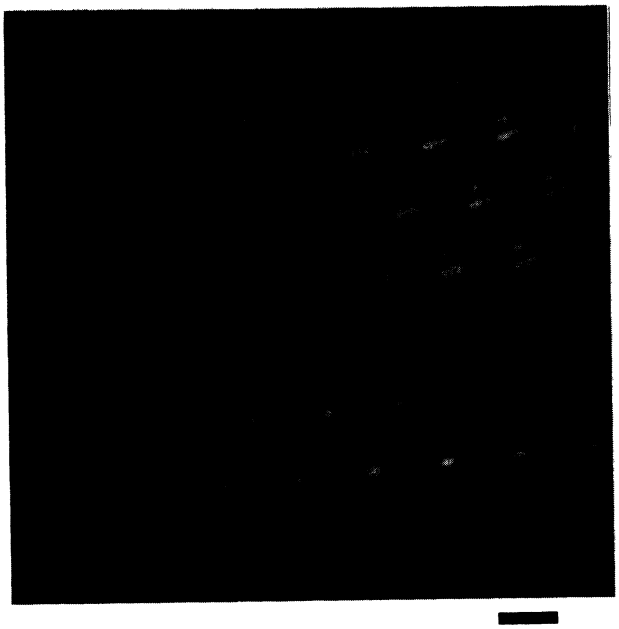

FIG. 4. Low-pass filtered STM image of 1*T*-$TaS_2$ in the *NC* phase. The bar below the picture is 10 Å. Notice the gradual variation of the atomic lattice structure superimposed on the CDW maximum indicating that the picture is not of a commensurate domain. The image was taken at 295 K with 4-nA tunneling current and the sample biased at −0.25 mV.

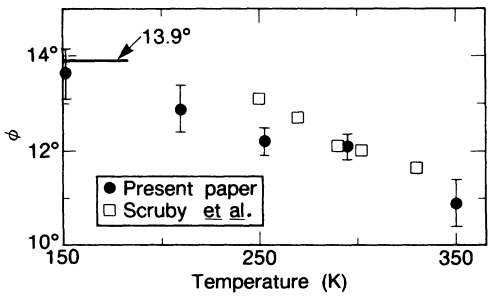


FIG. 5. Locally measured angle, $\phi$, of the CDW relative to the atomic lattice: For a detailed description of the angle measurement see the Appendix. The point at 143 K is in the *C* phase and is equal to 13.9° to within our estimated error. The remaining points are in the *NC* phase and are always less than the commensurate angle of 13.9°.

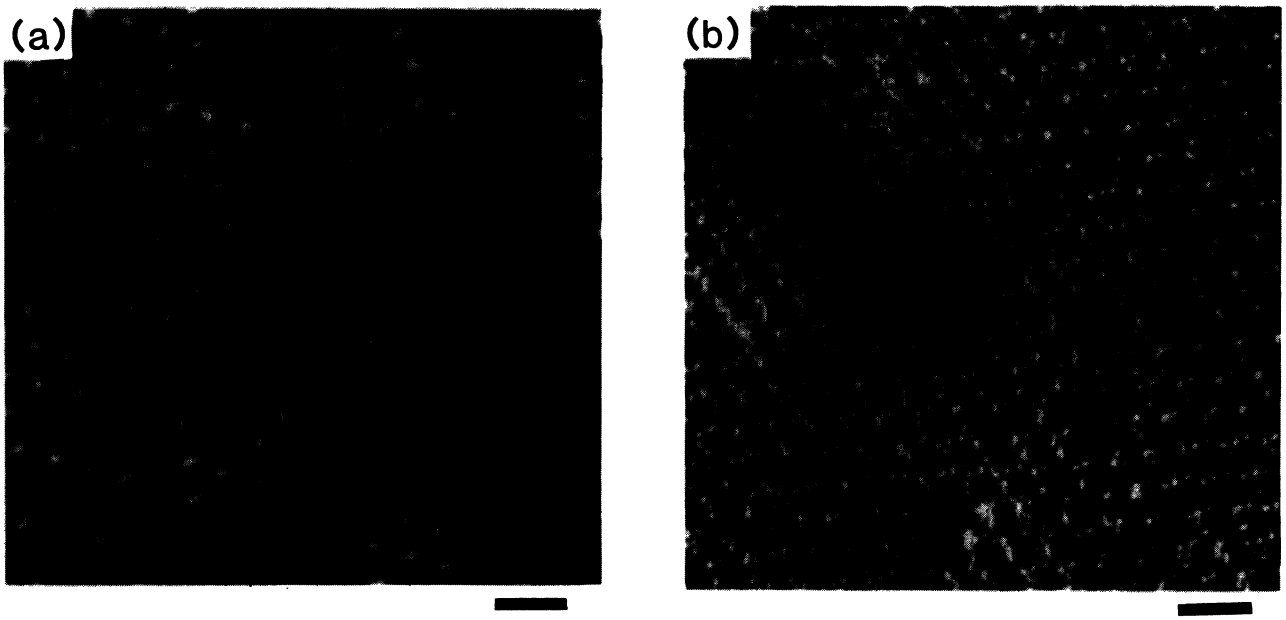


FIG. 6. 1$T$-$TaS_2$ in the *NC* phase showing variations in apparent amplitude of the CDW. The bars below the pictures are 25 Å. (a) Image taken at 251 K in a $N_2$ atmosphere with 7-nA tunneling current and $-10$ mV bias applied to the sample. Several extended areas of the image appear to have an anomalously strong CDW compared to the rest of the image. (b) Image taken at 210 K with the sample immersed in liquid $n$-pentane with a 4-nA tunneling current and the sample biased at $+0.25$ mV. Here there appear to be very localized areas where the CDW is enhanced or suppressed.

configuration of the atoms superimposed on the CDW maxima varies slightly from one maxima to the next across both pictures.

A more rigorous test for commensurate domains is provided by a local measurement of the angle of the CDW relative to the lattice. We usually take images that are from 50 to 100 Å. Thus, if commensurate domains of the size predicted exist (70 to 85 Å in diameter), we should be able to take an image almost completely within one domain. A large sampling of images should yield at least one or two which exhibit the commensurate angle, $\phi = 13.9°$, in all three directions. This is not what we found. On the contrary, in analyzing 10 images of samples in the *NC* phase we found none in which the angle in even one direction approached 13.9° (see the Appendix for a detailed description of how the angle was mea-

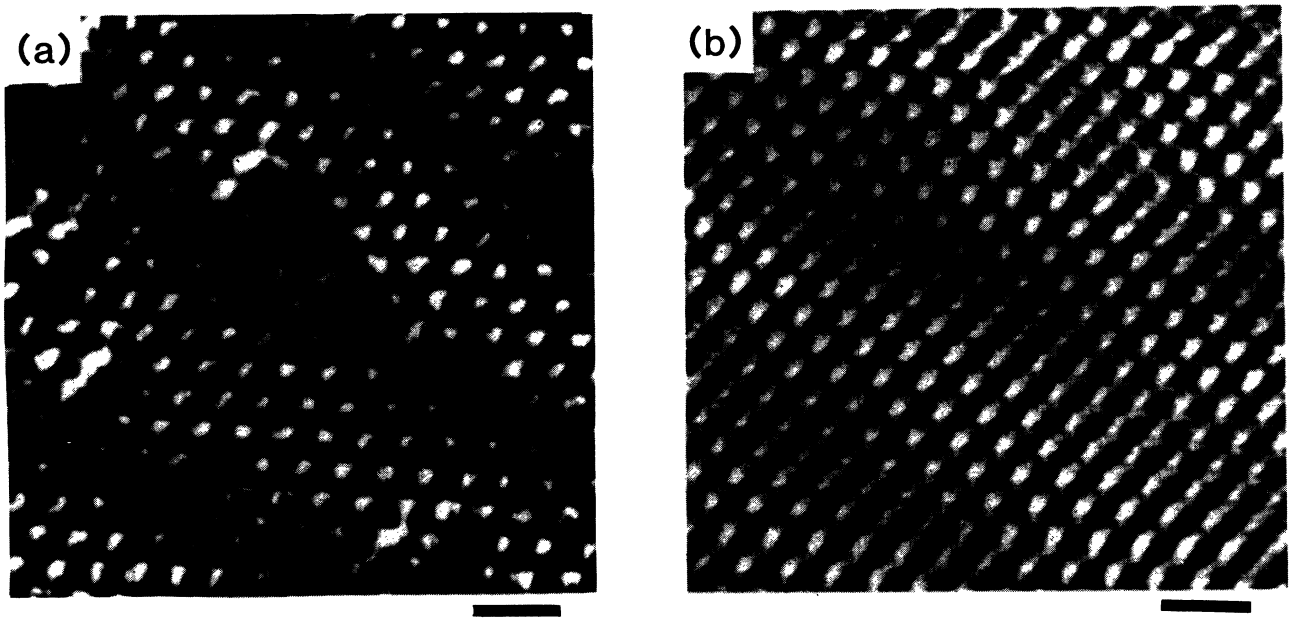


FIG. 7. 1$T$-$TaSe_2$ in the $T$ phase. The CDW is clearly observed in long narrow domains separated by walls where the CDW amplitude is suppressed. The bars below each picture are 25 Å. (a) Image taken at 225 K while the sample was immersed in $n$-pentane with 5-nA tunneling current and the sample biased at $+20$ mV. (b) Image taken on a different sample at 237 K while the sample was immersed in $n$-pentane with a 3-nA tunneling current and the sample biased at $-4$ mV.

sured). Moreover, if the discommensurate domain model were correct, we would expect the average angles of different pictures to vary significantly, depending on whether the image was centered on a domain or on a boundary between domains. All the images we analyzed exhibited very similar average angles, however, as shown in Fig. 5 by the small standard deviations on our data points.

It should be mentioned that although we do not see the domains predicted by Nakanishi *et al.* where $\phi$, the angle of the CDW, defines the domain, and where the amplitude of the CDW is predicted to vary only at these domain walls, we do see variations in the apparent amplitude of the CDW in the *NC* phase as well as in all the other phases. For example, in Fig. 6(a), an image taken at 250 K in the *NC* phase, one can see large areas where the CDW appears much stronger than in others. In Fig. 6(b), the enhanced or depressed areas appear to be more localized. We found these areas where the CDW is enhanced or suppressed to be randomly distributed throughout the sample. They appeared in all the samples we tested including samples in the *C* phase where they appeared most frequently and were extremely stable from scan to scan. We suggest these variations are due to defects, impurities, or surface contamination.

### D. *T* phase

After our thorough study of the *NC* phase where we found no evidence of the predicted domain structure, we were surprised to find domains in the *T* phase similar to those predicted. In four out of five extensive sets of images obtained on three samples we found long narrow sections in which the CDW amplitude is large. Figure 7 shows two typical examples of this structure, taken on

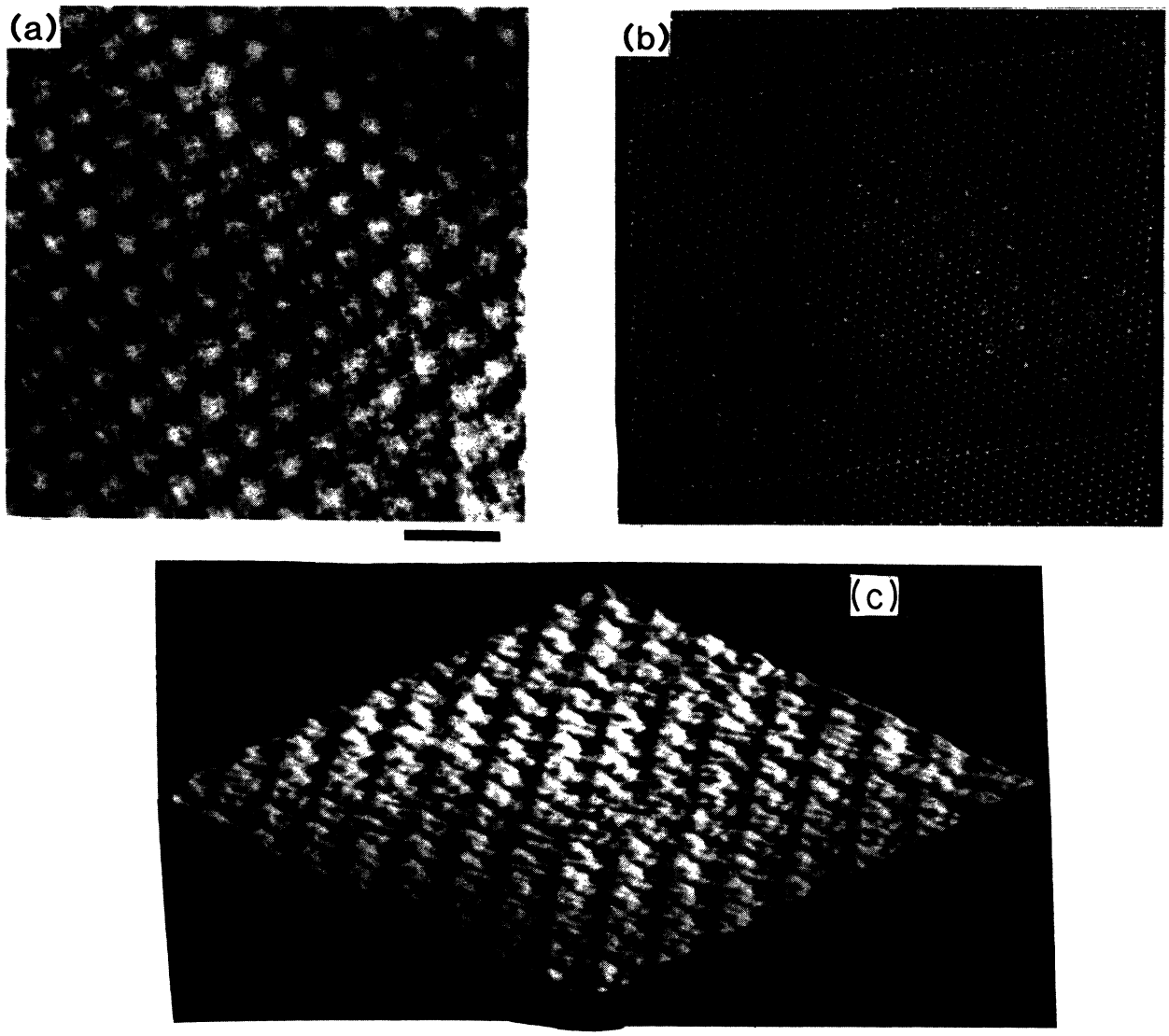


FIG. 8. 1*T*-$TaS_2$ in the *T* phase. (a) Raw data: Image was take at 236 K with the sample immersed in *n*-pentane; tunneling current was 5 nA and the sample was biased at $-4$ mV. The bar below the image is 25 Å. (b) Computer analysis of (a) showing the locations of the position of the CDW minimum inside the two domains. Notice the phase slip of one atomic lattice unit across the domain wall. This is most easily observed by viewing the model at a glancing angle along the direction of the CDW minimum. (c) Projected view of the data shown in (a).

different samples. In any one sample, the domain walls are found to run approximately parallel across the entire area of the surface we are able to sample ($\approx 1\ \mu m^2$). Inside any one of these domains the CDW maxima (or minima) appear to be almost identical, leading us to conclude that the CDW is commensurate inside the domain.

To determine the relationship of the CDW in one domain to that in an adjacent domain, we made a computer model of an image to clarify the CDW positions. We first generated a lattice image and used it to determine the best skewing transform (see Appendix). On top of this ideal lattice grid we then plotted the centers of the CDW minima. Figure 8(a) shows the raw data and Fig. 8(b) the computer image generated in this way. Viewing Fig. 8(b) at a glancing angle along the direction of the CDW minima rows, one sees that the commensurate CDW in the left domain has suffered a phase slip of one lattice spacing relative to the commensurate CDW in the center domain. This is further illustrated by Fig. 8(c) which is a projected view of Fig. 8(a). Here the commensurate domains are clearly visible as the three areas where the CDW has a larger amplitude. [In Fig. 8(b) only two of these domains were plotted.] The phase slip that occurs at the discommensuration is also clearly shown by the jogs that occur in the lines of CDW maxima. The structure seen in this picture is thus exactly that proposed by McMillan for discommensurate phases.[27]

The size of the observed domains does not agree as well with the theory. Although there is some difficulty in determining the exact location of the domain walls, we estimate the long narrow domains to be approximately 60–70 Å across for samples at 234 K. From their own x-ray diffraction data and the theory by Nakanishi and Shiba,[26] Tanda and Sambongi calculate this distance at 225 K to be about 40 Å.[9] However, the orientation of the stripe domains relative to the CDW is in good agreement. We measure this angle to be $\approx 26°$, while Tanda and Sambongi report it to be 28.3°.[9]

## V. CONCLUSION

We have observed the CDW in 1$T$-$TaS_2$ in all four phases where it is present. Since the atomic beam diffraction[22] and low-energy electron diffraction[21] experiments indicate strongly that the CDW structure at the surface has the same periodicity as the bulk CDW, we believe that our findings also hold for the bulk CDW. This is supported by the very good agreement between the transition from the $I$ to $NC$ phase observed at the surface with the STM and the bulk transition as reflected in the resistance measurement.

We found the incommensurate CDW in the $I$ phase and the commensurate CDW in the $C$ phase to be exactly as expected from diffraction data. We observed the nearly commensurate CDW in the $NC$ phase to be uniformly incommensurate with no apparent commensurate domain structure. By way of contrast, in the $T$ phase we found long narrow stripe domains very similar to those predicted for this phase by Nakanishi and Shiba[26] and described by Tanda and Sambongi.[9]

## ACKNOWLEDGMENTS

We would like to thank D. W. Abrahams, H. J. Mamin, and P. K. Hansma for useful discussions regarding the microscope design. This work was supported by the Director, Office of Energy Research, Office of Basic Energy Science, Materials Science Division of the U.S. Department of Energy, under Contract No. DE-AC03-76F00098, and by the Materials Science Center at Cornell University through National Science Foundation (NSF) Grants No. DMR-85-16616-A01. U.W. received support from the Deutsche Forschungsgemeinschaft. A.Z. acknowledges support from NSF Grants No. DMR-84-00041 and No. DMR-83-51678 and the Alfred P. Sloan Foundation. E.G. was supported by IBM.

## APPENDIX: DATA ANALYSIS

To measure the angle of rotation ($\phi$) of the CDW accurately with respect to the lattice we correct the raw STM images for distortion. This is a skewing of the image caused by a combination of slight inaccuracies in the settings of the scanning voltages, $x$ and $y$ drives which were not identical, and steady (time-independent) thermal drift. (Images obtained at temperatures well above room temperature also showed a curving of the image caused by time-dependent thermal drift.) We corrected the images so that the underlying atoms formed a perfect hexagonal array. To measure $\phi$ to better than 1°, it is important to perform these corrections as accurately as possible. This was achieved by using a lattice averaging technique to improve the precision with which the atomic locations are determined.

First we perform a 2D Fourier transform of the image. Figure 9(a) shows a typical image of 1$T$-$TaS_2$ taken at room temperature, and Fig. 9(b) shows its Fourier transform. Retaining only those spots which correspond to the atomic lattice and eliminating the remaining points in the Fourier transform, we obtain Fig. 9(d). When we transform these selected Fourier components back to real space, we obtain Fig. 9(c). We use this image to calculate the correct $2\times 2$ linear transform to map the lattice onto a perfect hexagonal structure as accurately as possible. To determine the locations of the CDW maxima as accurately as possible we generate a CDW image by choosing only the lowest-order spots in the Fourier transform and transforming those back to real space, as shown in Figs. 9(e) and 9(f). It is also possible to generate a filtered image by selecting both sets of points simultaneously [Figs. 9(g) and 9(h)].

Once we have calculated the correct skewing transform, we apply it to both the lattice and the CDW images. These two corrected images are used to measure the relative angle between rows of atoms and rows of CDW maxima. Because the correction is not perfect, the angle we measure between the CDW and the lattice is usually slightly different depending on which of the three equivalent directions along which we measure it. The differences in the angles in a single picture ranged from 0.1° to about 1°. However, the average of these three angles from many different pictures taken at the same tem-

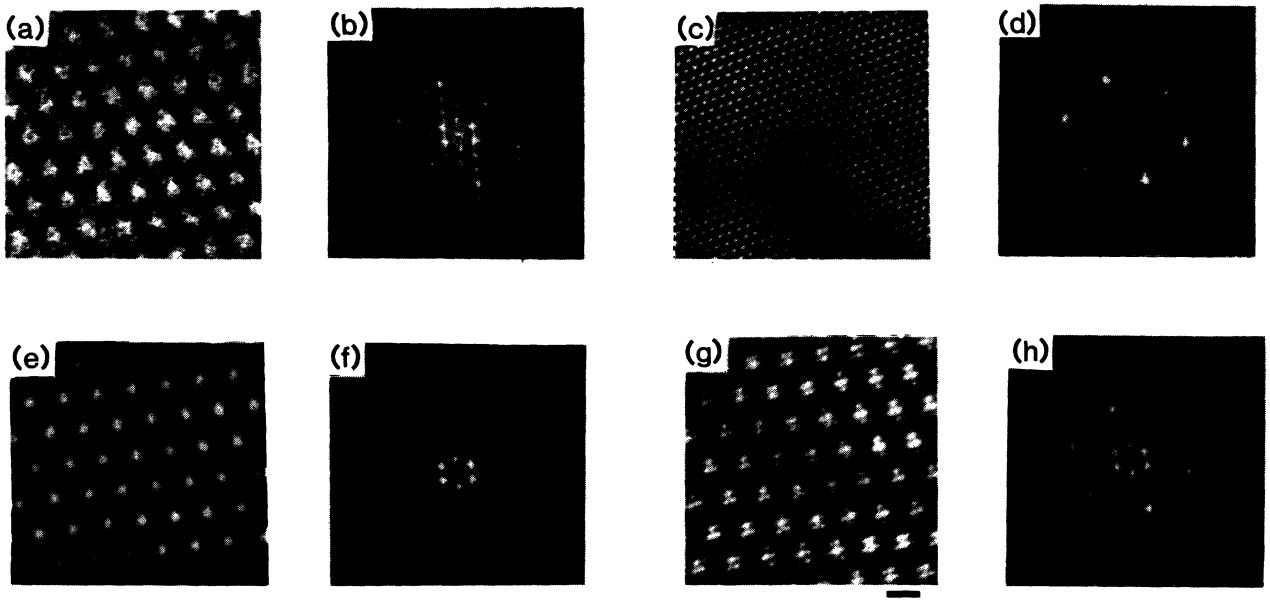


FIG. 9. Fourier filtering of an image of 1*T*-$TaS_2$ in the *NC* phase. The bar at the bottom of the series is 10 Å. (a) Raw data: Image was taken at 295 K with 4-nA tunneling current and the sample was biased at −0.25 mV. (b) Fourier transform of the raw data. (c) Lattice image obtained by selecting only the first-order lattice spots in the Fourier transform as shown in (d). (e) Image of the CDW generated by selecting only the lowest order CDW spots in the Fourier transform as shown in (f). (g) Highly filtered picture of the data generated by adding both (d) and (f) to obtain (h), and transforming back to real space.

perature was constant. For ten pictures taken at room temperature, the mean average angle was 12.06° and the standard deviation of the averages was only 0.2°. For this reason we believe that the differences in the measured angle in the different directions in a single picture were an artifact caused by our inability to create a perfect correction for the skewed data, and not a real aspect of the data.

*Present address: Deutsche Forschungs- und Versuchsanstalt für Luft- und Raumfahrt e.V., Postfach 906058, 5000 Köln 90, West Germany.

[1]J. A. Wilson, F. J. DiSalvo, and S. Mahajan, Adv. Phys. **24**, 117 (1975).
[2]G. Gruner and A. Zettl, Phys. Rep. **117**, 119 (1985).
[3]M. Barmatz, L. R. Testardi, and F. J. DiSalvo, Phys. Rev. B **12**, 4367 (1975); L. R. Testardi, *ibid.* **12**, 3849 (1975).
[4]R. V. Coleman, B. Drake, P. K. Hansma, and G. Slough, Phys. Rev. Lett. **55**, 394 (1985).
[5]B. Giambattista, A. Johnson, R. V. Coleman, B. Drake, and P. K. Hansma, Phys. Rev. B **37**, 2741 (1988).
[6]S. C. Bayliss, A. M. Ghorayeb, and D. R. P. Guy, J. Phys. C **17**, L533 (1984).
[7]O. Sezerman, A. M. Simpson, and M. H. Jericho, Solid State Commun. **36**, 737 (1980).
[8]T. Haga, Y. Abe, and Y. Okwamoto, Phys. Rev. Lett. **51**, 678 (1983).
[9]S. Tanda and T. Sambongi, Synth. Methods **11**, 85 (1985); S. Tanda, T. Sambongi, T. Tani, and S. Tanaka, J. Phys. Soc. Jpn. **53**, 476 (1984).
[10]A. Suzuki, M. Koizumi, and M. Doyama, Solid State Commun. **53**, 201 (1985).
[11]A. Suzuki, R. Yamamoto, M. Doyama, H. Mizubayashi, S. Okuda, K. Endo, and S. Gonda, Solid State Commun. **49**, 1173 (1984).
[12]T. Tani and S. Tanaka, J. Phys. Soc. Jpn. **53**, 1790 (1984); T. Tani, K. Okajima, T. Itoh, and S. Tanaka, Physica B + C **105B**, 127 (1981).
[13]R. Inada, Y. Onuki, and S. Tanuma, Physica B + C **99B**, 188 (1980); Phys. Lett. **69A**, 453 (1979).
[14]R. Brouwer and F. Jellinek, Physica B + C **99B**, 51 (1980).
[15]C. B. Scruby, P. M. Williams, and G. S. Parry, Philos. Mag. **31**, 255 (1975).
[16]L. D. Chapman and R. Colella, Phys. Rev. B **32**, 2233 (1985).
[17]M. Kuwabara, M. Tomita, H. Hashimoto, and H. Endoh, Phys. Status Solidi A **96**, 39 (1986).
[18]J. van Landuyt, G. van Tandeloo, and S. Amelinckx, Phys. Status Solidi A **26**, 359 (1974); **26**, 585 (1974); **36**, 757 (1976); **42**, 565 (1977); J. van Landuyt, Physica B + C **99B**, 12 (1980).
[19]K. K. Fung, J. W. Steeds, and J. A. Eades, Physica B + C **99B**, 47 (1980); D. M. Bird, D. J. Eaglesham, R. L. Withers, S. McKernan, and J. W. Steeds, in *Proceedings of the International Conference on Charge Density Waves in Solids, 1984, Budapest* (Springer-Verlag, Berlin, 1985), pp. 23–32.
[20]R. L. Withers and J. W. Steeds, J. Phys. C **20**, 4019 (1987).
[21]B. J. Mrstik, R. Kaplan, T. L. Reineke, M. Van Hove, and S. Y. Tong, Nuovo Cimento **38**, 387 (1977).
[22]P. Cantini, G. Boato, and R. Corella, Physica B + C **99B**, 59 (1980).
[23]G. van Tendeloo, J. van Landuyt, and S. Amelinckx, Phys. Status Solidi A **64**, K105 (1981).
[24]Y. Yamada and H. Takatera, Solid State Commun. **21**, 41 (1977); A. Yamamoto, Phys. Rev. B **27**, 7823 (1983).

[25]K. Nakanishi, H. Takatera, Y. Yamada, and H. Shiba, J. Phys. Soc. Jpn. **43**, 1509 (1977); K. Nakanishi and H. Shiba, *ibid.* **43**, 1893 (1977).
[26]K. Nakanishi and H. Shiba, J. Phys. Soc. Jpn. **53**, 1103 (1984).
[27]W. L. McMillian, Phys. Rev. B **14**, 1496 (1976).
[28]H. P. Hughes and R. A. Pollak, Commun. Phys. **1**, 61 (1976).
[29]C. H. Chen, J. M. Gibson, and R. M. Fleming, Phys. Rev. Lett. **47**, 723 (1981); Phys. Rev. B **26**, 184 (1982); K. K. Fung, S. McKernan, J. W. Steeds, and J. A. Wilson, J. Phys. C **14**, 5417 (1981); T. Onozuka, N. Otuska, and H. Sato, Phys. Rev. B **34**, 3303 (1986); Y. Koyama, Z. P. Zhang, and H. Sato, *ibid.* **36**, 3701 (1987).
[30]W. J. Kaiser and R. C. Jaklevic, Surf. Sci. **181**, 55 (1987).
[31]B. Drake, R. Sonnefeld, J. Schneir, and P. K. Hansma, Surf. Sci. **181**, 92 (1987).
[32]G. Binnig and D. P. E. Smith, Rev. Sci. Instrum. **57**, 1688 (1986).
[33]B. Drake, R. Sonnenfeld, J. Schneir, P. K. Hansma, G. Slough, and R. V. Coleman, Rev. Sci. Instrum. **57**, 441 (1986).
[34]A. Bryant, D. P. E. Smith, and C. F. Quate, Appl. Phys. Lett. **48**, 832 (1986).
[35]S. Noutomi, T. Futatsugi, M. Naito, and S. Tanaka, Solid State Commun. **50**, 181 (1984).

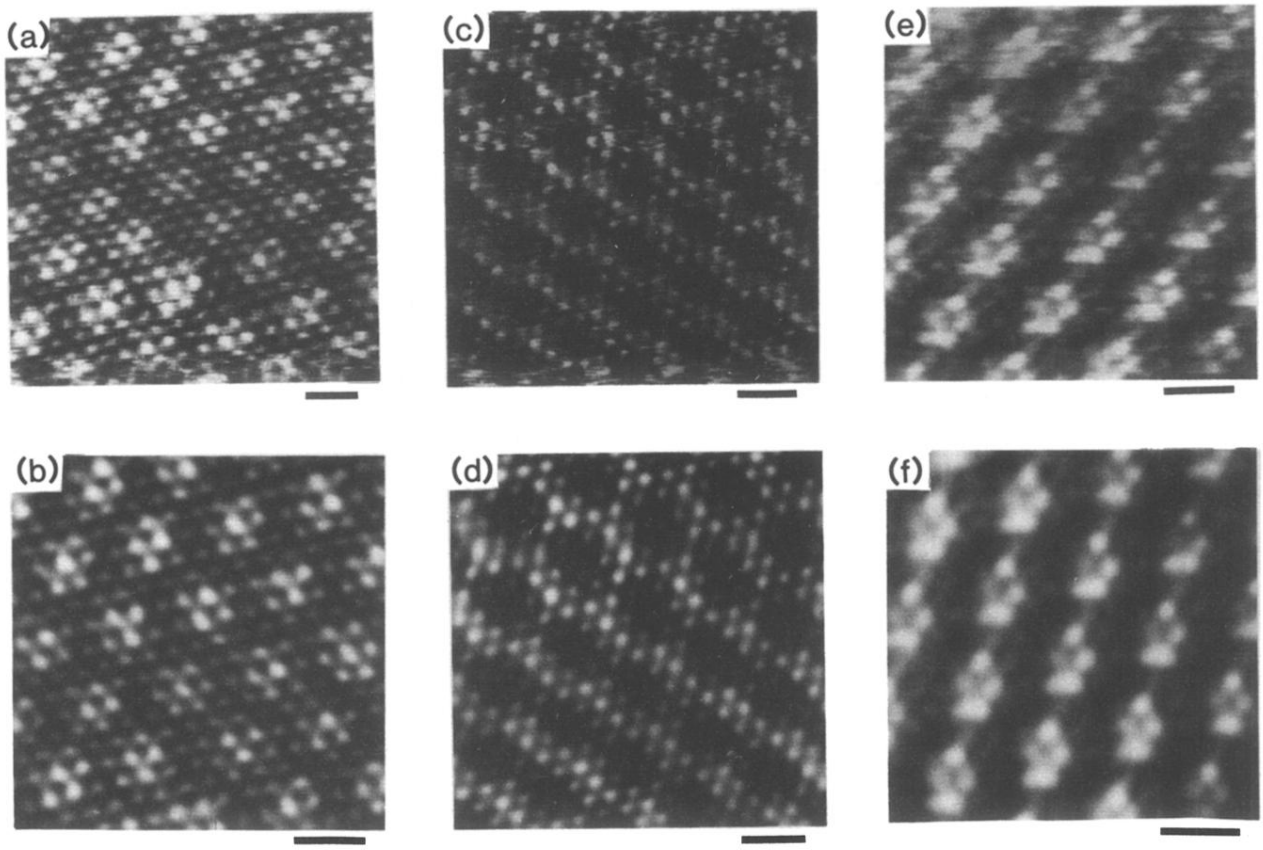


FIG. 3. Raw data and filtered images of $1T$-$TaS_2$. The bar below each picture is 10 Å. (a) Raw and (b) low-pass filtered image taken at 360 K in the *I* phase. The image was taken in air with 7.5-nA tunneling current and the sample biased at $-4.8$ mV. (c) Raw and (d) filtered image taken at 350 K just after the transition to the *NC* phase. The sample was under silicone oil and the image was taken with 5-nA tunneling current and the sample biased at $-13$ mV. (e) Raw and (f) filtered image taken at 143 K in the *C* phase. The sample was immersed in *n*-pentane and the image was taken with 5-nA tunneling current and the sample biased at $+20$ mV.

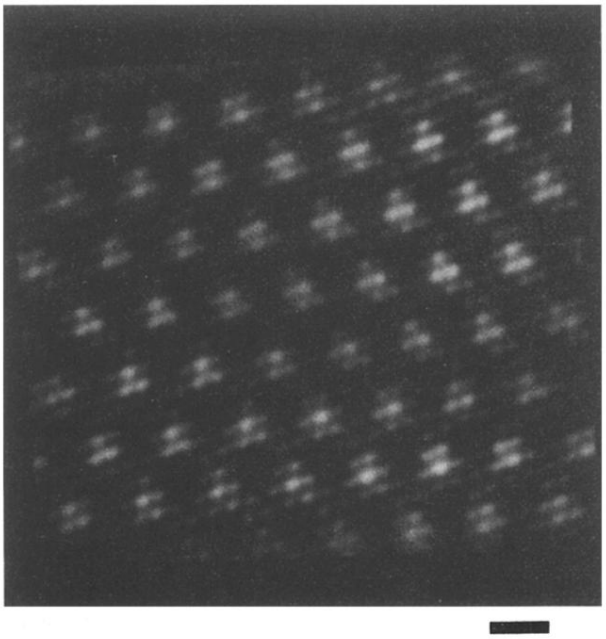

FIG. 4. Low-pass filtered STM image of $1T$-$TaS_2$ in the *NC* phase. The bar below the picture is 10 Å. Notice the gradual variation of the atomic lattice structure superimposed on the CDW maximum indicating that the picture is not of a commensurate domain. The image was taken at 295 K with 4-nA tunneling current and the sample biased at $-0.25$ mV.

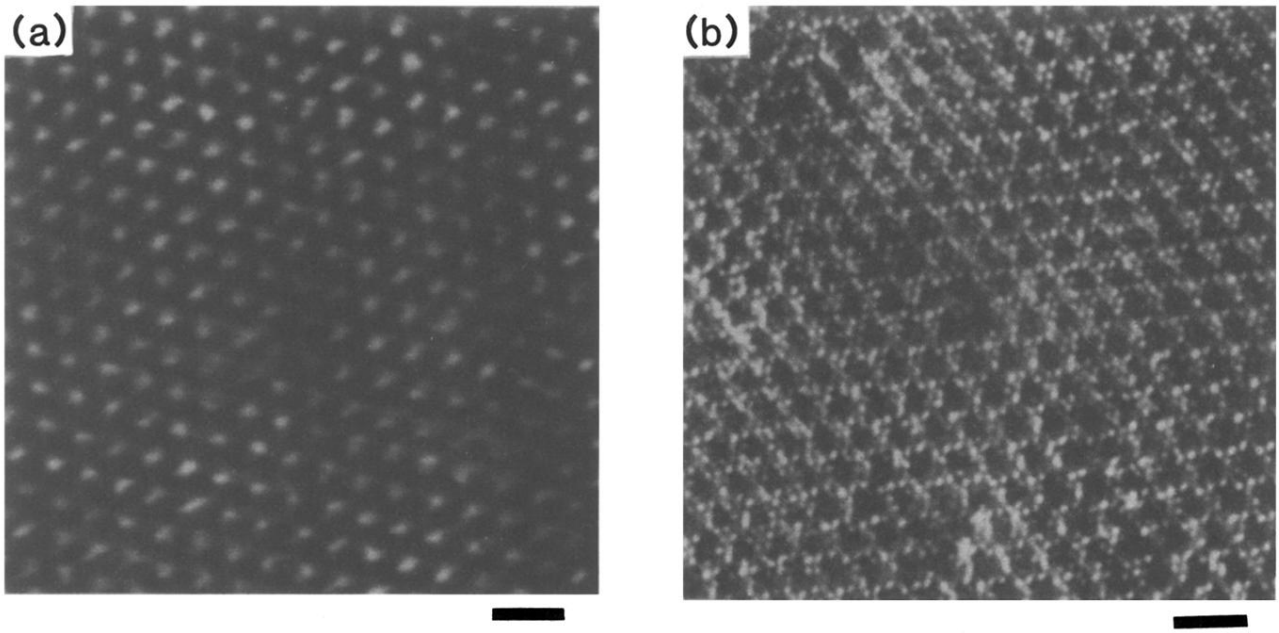


FIG. 6. 1*T*-$TaS_2$ in the *NC* phase showing variations in apparent amplitude of the CDW. The bars below the pictures are 25 Å. (a) Image taken at 251 K in a $N_2$ atmosphere with 7-nA tunneling current and $-10$ mV bias applied to the sample. Several extended areas of the image appear to have an anomalously strong CDW compared to the rest of the image. (b) Image taken at 210 K with the sample immersed in liquid *n*-pentane with a 4-nA tunneling current and the sample biased at $+0.25$ mV. Here there appear to be very localized areas where the CDW is enhanced or suppressed.

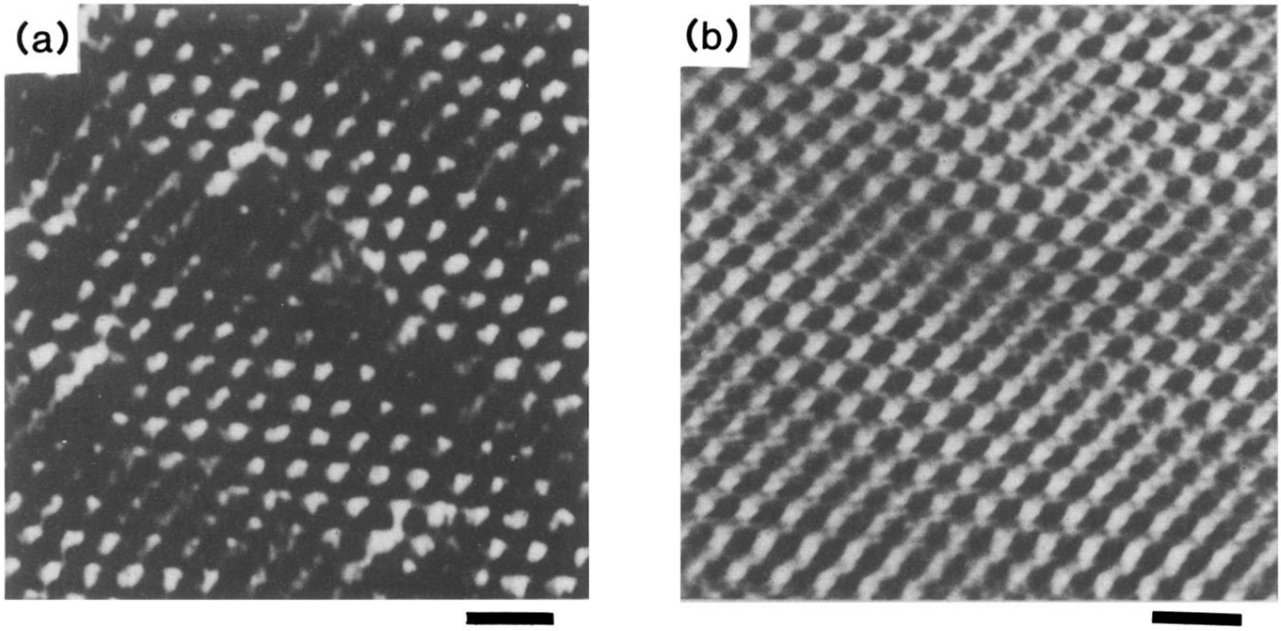


FIG. 7. $1T$-$TaSe_2$ in the $T$ phase. The CDW is clearly observed in long narrow domains separated by walls where the CDW amplitude is suppressed. The bars below each picture are 25 Å. (a) Image taken at 225 K while the sample was immersed in $n$-pentane with 5-nA tunneling current and the sample biased at $+20$ mV. (b) Image taken on a different sample at 237 K while the sample was immersed in $n$-pentane with a 3-nA tunneling current and the sample biased at $-4$ mV.

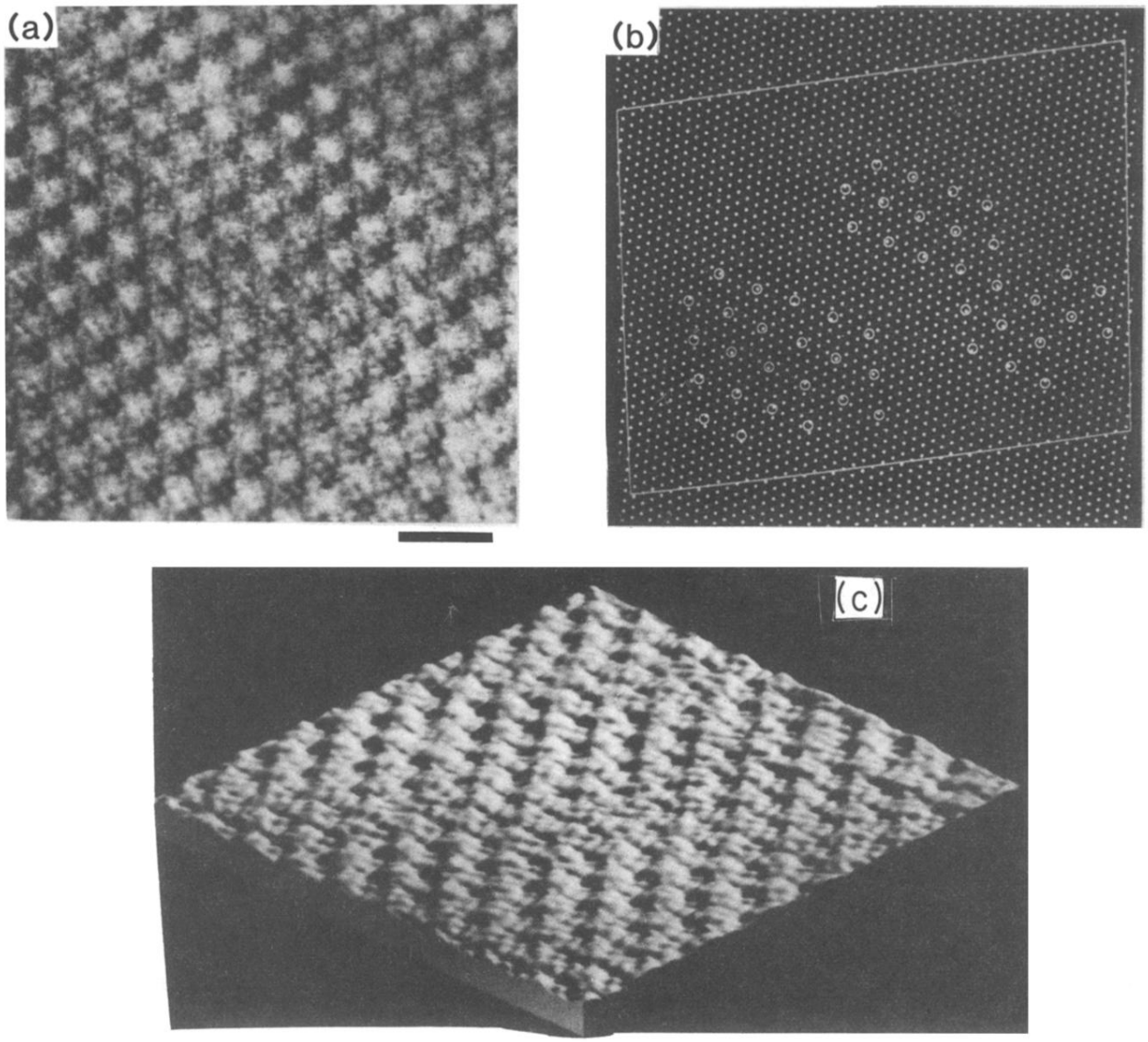


FIG. 8. $1T$-$TaS_2$ in the $T$ phase. (a) Raw data: Image was take at 236 K with the sample immersed in $n$-pentane; tunneling current was 5 nA and the sample was biased at $-4$ mV. The bar below the image is 25 Å. (b) Computer analysis of (a) showing the locations of the position of the CDW minimum inside the two domains. Notice the phase slip of one atomic lattice unit across the domain wall. This is most easily observed by viewing the model at a glancing angle along the direction of the CDW minimum. (c) Projected view of the data shown in (a).

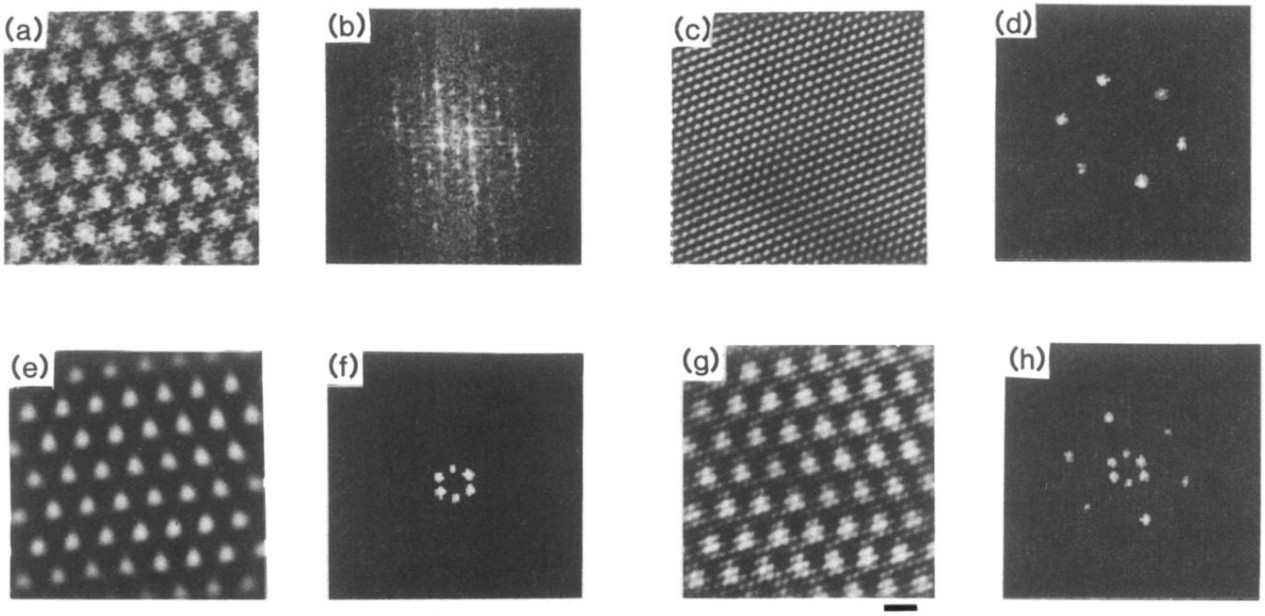


FIG. 9. Fourier filtering of an image of 1*T*-$TaS_2$ in the *NC* phase. The bar at the bottom of the series is 10 Å. (a) Raw data: Image was taken at 295 K with 4-nA tunneling current and the sample was biased at $-0.25$ mV. (b) Fourier transform of the raw data. (c) Lattice image obtained by selecting only the first-order lattice spots in the Fourier transform as shown in (d). (e) Image of the CDW generated by selecting only the lowest order CDW spots in the Fourier transform as shown in (f). (g) Highly filtered picture of the data generated by adding both (d) and (f) to obtain (h), and transforming back to real space.